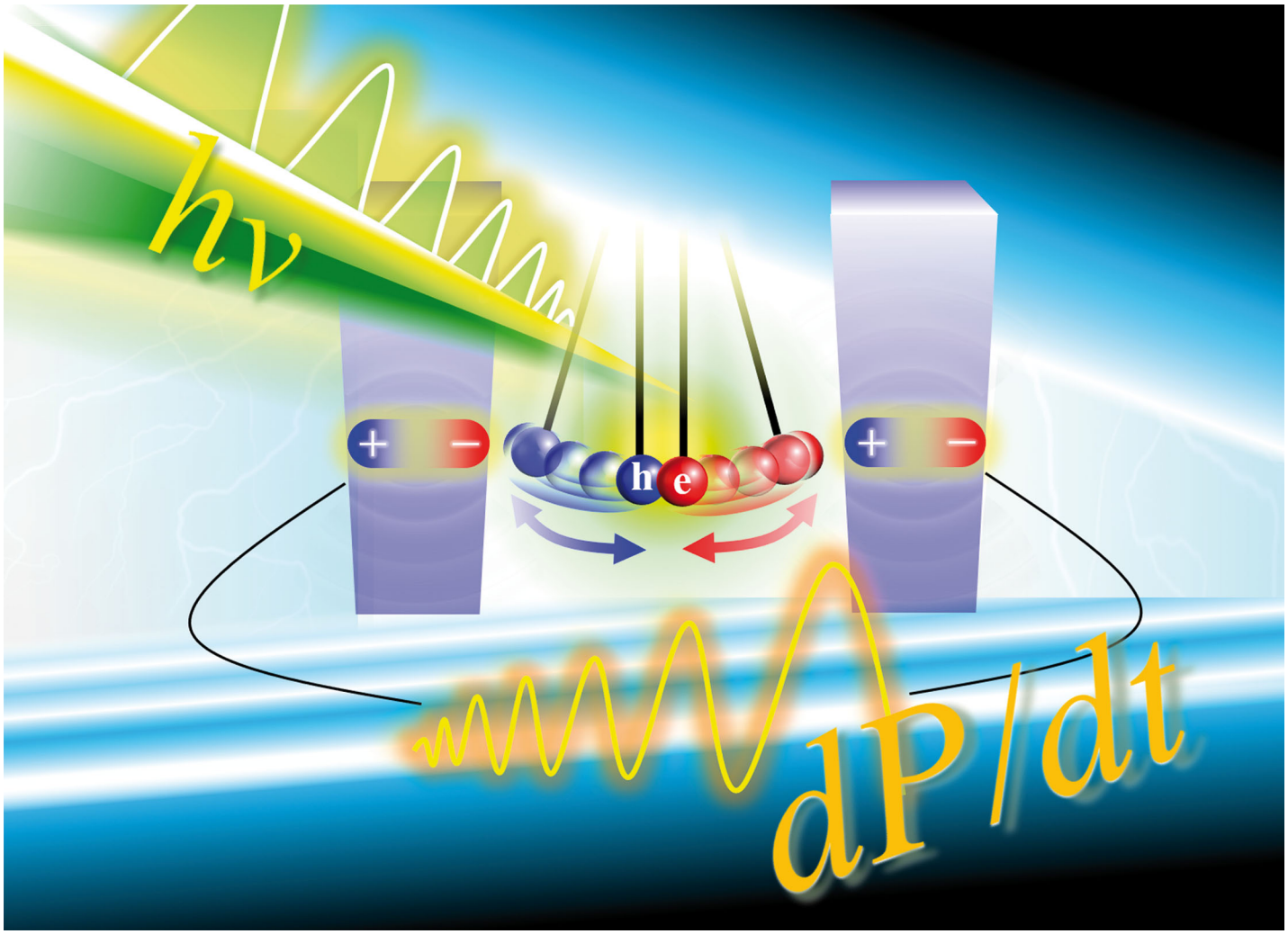

Showcasing Research from the Group of Professor Kunio Awaga at Nagoya University, Japan.

Rate-determining process in MISIM photocells for optoelectronic conversion using photo-induced pure polarization current without carrier transfer across interfaces

We investigated [metal|insulator|semiconductor|insulator|metal] (MISIM) photocells, a recently developed architecture for high-speed organic photodetectors. The electric polarization in the S layer, induced by modulated light illumination, propagates into the outer circuit as a polarization current through the I layers without any carrier transfer across the interfaces. The present results reveal a common rate-determining process caused by an imbalance between a slow depolarization in the dark and a fast polarization under illumination.

As featured in:

See Seiya Yokokura, Kunio Awaga *et al.*, *Phys. Chem. Chem. Phys.*, 2019, **21**, 13440.

ROYAL SOCIETY OF CHEMISTRY | Celebrating IYPT 2019

rsc.li/pccp

Registered charity number: 207890

PCCP

PAPER

View Article Online
View Journal | View Issue

Cite this: *Phys. Chem. Chem. Phys.*, 2019, **21**, 13440

Rate-determining process in MISIM photocells for optoelectronic conversion using photo-induced pure polarization current without carrier transfer across interfaces†

Akihiro Tomimatsu,[a] Seiya Yokokura,*[b] Louisa Reissig,[c] Simon Dalgleish,[ad] Michio M. Matsushita[a] and Kunio Awaga*[a]

Received 2nd March 2019,
Accepted 16th April 2019

DOI: 10.1039/c9cp01221d

rsc.li/pccp

Recently, we proposed a [metal|insulator|semiconductor|insulator|metal] (MISIM) photocell, as a novel architecture for high-speed organic photodetectors. The electric polarization in the S layer, induced by modulated light illumination, propagates into the outside circuit as a polarization current through the I layers, without any carrier transfer across the interfaces. In the present work, we examined the MISIM photocells consisting of zinc-phthalocyanine(ZnPc)-C_{60} bilayers for the S layer and Parylene C for the two I layers, to understand the fundamental aspects of the MISIM photocells, such as current polarity and modulation-frequency dependence. It was found that, in such devices, the current polarity was primarily determined by the polarization in the S layer, which was induced by the donor–acceptor charge-transfer upon illumination. Furthermore, the ON and OFF current, which appeared in the periods of illumination-on and -off, respectively, exhibited significantly different dependence on the modulation frequency. This was well-explained by an imbalance between a quick polarization in the S layer during illumination and its slow relaxation in the dark.

1. Introduction

Organic optoelectronics devices have received attention recently by virtue of their low cost, light weight, and ease of fabrication.[1–4] However, attempts to utilize organic materials in these devices generally encounter the most significant problem with organic materials: their poor mobility. Due to this and to an imbalance between hole and electron mobilities, space charges are always produced in organic photocells such as organic solar cells[5–7] and photodetectors,[8–10] thus limiting the photocurrent in these devices. However, it is also notable that photogenerated space charges can boost optoelectronic conversion through the generation of a highly efficient transient photocurrent.

We thus developed a new light-harvesting principle for optoelectronic conversion based on a [metal (M)|organic insulator (I)|organic semiconductor (S)|metal (M)] (MISM) structure.[11–16] As shown in Fig. 1(a), illumination induces photocarriers in the organic S layer after charge separation, followed by charge transfer to the neighboring electrode (M layer). This generates a transient photocurrent in the outside circuit and results in polarization P in the I layer. This process is identical to those in photocapacitors.[17,18]

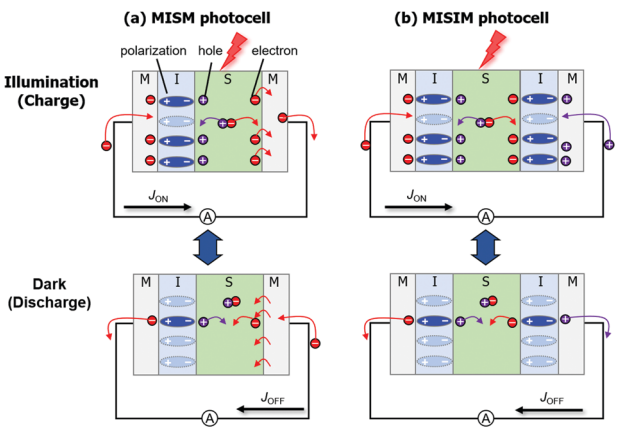

Fig. 1 Comparison between the optoelectronic conversions in the MISM (a) and MISIM (b) photocells.

[a] *Department of Chemistry & Integrated Research Consortium on Chemical Sciences (IRCCS), Nagoya University, Furo-cho, Chikusa-ku, Nagoya 464-8602, Japan. E-mail: awaga.kunio@b.mbox.nagoya-u.ac.jp*
[b] *Venture Business Laboratory (VBL), Nagoya University, Furo-cho, Chikusa-ku, Nagoya 464-8602, Japan. E-mail: yokokura.seiya@b.mbox.nagoya-u.ac.jp*
[c] *Institute of Experimental Physics, Freie Universität Berlin, Arnimallee 14, 14195 Berlin, Germany*
[d] *Institute for Advanced Research, Nagoya University, Furo-cho, Chikusa, 464-8601 Nagoya, Japan*

† Electronic supplementary information (ESI) available: Experimental details, frequency dependence of photocurrent measurement with different electrodes and frequency dependence of polarization. See DOI: 10.1039/c9cp01221d

However, since the I layer directly faces the S layer in MISM photocells, the polarization in the I layer can synergistically magnify the charge separation in the S layer and make the transient photocurrent anomalous. When the illumination stops, the polarization in the I layer gradually collapses, inducing a reverse transient current in the outside circuit. Therefore, charge and discharge in the I layer of an MISM photocell take place under illumination and in the dark, respectively, and the current density in the outside circuit can be expressed as a polarization current, namely $J = dP/dt$, where t is time. The obtained performance is highly applicable to pulsed light detection in many systems such as optical communication devices and image sensors. Since this optoelectronic conversion mechanism, utilizing polarization currents, does not necessarily require high mobility in the S layer, the strong and tunable absorption profiles of organic materials make them ideal targets. To date, such MISM photodetectors, with bandwidths up to 1 MHz operating at communication-relevant wavelengths, could be fabricated, even for low-mobility semiconductors,[12] and with a better-optimized molecular design, higher speeds can be anticipated. Furthermore, the use of ionic liquids (ILs) as insulating layers has significantly increased the responsivity of these IL-MISM devices to 272 mA W^{-1},[13] comparable to commercially available silicon photodiodes, with high stability and high reproducibility. However, MISM photocells suffer from a responsivity/bandwidth trade-off: a large capacitance C in the I layer magnifies the transient photocurrent but also slows the response.[11]

Recently, we proposed asymmetric MISIM photocells to overcome this weak point of MISM devices.[19] By using both large- and small-capacitance insulating materials for the I and I′ layers in the MISI′M cells ($C_I \gg C_{I'}$), a strong electric field at the S|I interface is largely maintained, supporting efficient charge separation across the active layer, while the series capacitance C_{tot} of the device is significantly reduced according to I′ (since $1/C_{tot} \approx 1/C_{I'}$). Thus, the bandwidth can be expected to approach those of MISM devices based on low-k dielectrics. Although the MISM structure requires a carrier transfer across the S|M interface, the photocurrent response in the MISIM photocells is generated purely by the polarization of the semiconductor layer under illumination, without carrier injection from the electrode(s), thereby eliminating contact resistance effects that can additionally reduce the bandwidth and the responsivity of MISM devices. Even though the polarizations are limited within each domain, namely to the I, S, and I′ layers, and there is no carrier transfer across the interfaces, the MISIM photocells can induce a photocurrent in the outside circuit (Fig. 1(b)).

It is worth noting here that inorganic MISIM photocells with thin metal oxide films as the I layers have been reported,[20,21] but in those studies, the roles of the I layers have been to reduce the dark current across the photocells under reverse bias and thereby to improve their detectivity. Therefore, the operating principle is distinct from that of the polarization-current photocells described above. It is also notable that AC light-emitting diodes (LEDs) with MISIM structures, which convert AC voltage to modulated emission, have already been reported.[22–24] The optoelectronic conversion in the present MISIM photocells can be regarded as a reverse process of such AC LEDs.

In the present study, we investigated fundamental aspects of MISIM photocells with stable Parylene C (PC) insulating layers, which are widely used for their excellent properties such as chemical inertness, pinhole-free feature, ease of microfabrication, biocompatibility, and flexibility. While the magnitude of photoresponse is inevitably reduced by using symmetric low-k dielectrics, compared to IL-based devices, the absence of specific chemical interactions at the S|I interfaces (possibly leading to doping, dissolution or pre-polarization) greatly facilitates the interpretation of the results. We discuss the correlation between the polarization in the S layer and the photocurrent in the outside circuit, with an eye toward developing the performance of MISIM photocells.

2. Experimental

2.1 Device fabrication

ZnPc (zinc-phthalocyanine) and C_{60} were purchased from Sigma Aldrich and purified by vacuum sublimation. ITO patterned substrates were cleaned by ultrasonication (0.5% Helmanex III solution, acetone–2-propanol, 15 min each). After drying in an oven, UV/ozone cleaning was performed (Bioforce Nanosciences ProCleanerPLUS, 30 min). MISIM′ photocells with M = ITO, I = Parylene C (PC), S = bilayer of ZnPc and C_{60}, and M′ = Au, Cu, and Ag, were prepared by vapor deposition in a vacuum ($\sim 2 \times 10^{-4}$ Pa). The evaporation rates of the organic and metal materials are 0.2–0.3 Å s^{-1} and 1–2 Å s^{-1}, respectively. Parylene-C (SCS) with the thickness of 230 nm was deposited using a Specialty Coating Systems PDS2010 deposition unit. The S layer consisted of ZnPc (25 nm) and C_{60} (25 nm). The film thickness was monitored by using a QCM, which was calibrated by a white-light interferometric microscope (BW-S501, Nikon Instruments) for a scratched film.

2.2 Photocurrent measurements

The measurement setup and device structure are illustrated in Fig. S1 (ESI†). The photocells were irradiated from the ITO side by a pulse laser ($\lambda_{max} = 639 \pm 10$ nm, OPG-1000PL-640, Scientex) with an output power density of 40 mW cm^{-2} (100%), modulated by a function generator (FG-273, Texio) at various frequencies (1 kHz–1 MHz) under a zero-bias voltage. The shape of the laser spot is an ellipse with major and minor axes of approximately 4 and 2.5 mm, respectively. The device area (2×2 mm) is fully covered by the spot. In all cases, the generated photocurrent response was amplified using a high-speed transimpedance amplifier (Femto DHPCA100) and visualized on an oscilloscope (Tektronix TDS5104B) in average mode. We confirmed that the modulation of light (on and off) occurred completely in the frequency range of 1 kHz–1 MHz by measuring the photoresponse of SiPD (Fig. S2, ESI†).

3. Results and discussion

3.1 Polarity of photocurrent in MISIM photocells

We investigated the controlling factors that govern the polarity of the photocurrent in MISIM photocells using two kinds of

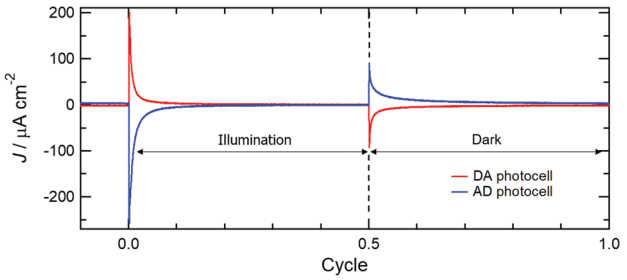

Fig. 2 Photocurrent in the DA (red) and AD photocell (blue).

device structures: [ITO|PC|ZnPc|C_{60}|PC|Au] (DA photocell) and [ITO|PC|C_{60}|ZnPc|PC|Au] (AD photocell). The red curve in Fig. 2 shows the photocurrent transient of a DA photocell induced by the irradiation of a pulse laser at 639 nm from the ITO side, with an output power density of 40 mW cm^{-2} and an on–off moderation frequency of 10 kHz. The DA photocell clearly exhibits a positive transient current under illumination, which means a current from the ITO electrode to the Au electrode in the external circuit. This current is consistent with the polarization induced by the electron transfer from ZnPc to C_{60} under illumination. In the dark, the DA photocell exhibits a negative transient current, which is considered to be caused by the discharge process. Even though the active layer is isolated from the electrodes by the solid-state PC layers, the [ITO|PC|ZnPc|C_{60}|PC|Au] photocell can produce a polarization current with a photoresponsivity of $\sim$5 mA W^{-1} at the positive peak value of the transient current. The blue curve in Fig. 2 shows the photocurrent of the [ITO|PC|C_{60}|ZnPc|PC|Au] (AD) photocell; the polarity of the transient photocurrent is reversed compared to that of the DA photocell, showing a slightly larger photoresponsivity of $\sim$6 mA W^{-1}. It is clear that the polarity of the transient photocurrent on the MISIM photocells is determined by the photo-induced polarization in the S layer at least when they are sandwiched between ITO and Au electrodes.

The energy level alignment of the work functions of ITO and Au,[25,26] the HOMO in ZnPc, and the LUMO in C_{60} together suggest that the charge separation in the AD photocell is energetically more favorable than that in the DA photocell. However, there is only a minimal difference between them in photocurrent intensity (Fig. 2). We also investigated the effects of a Ag and Cu electrode, instead of Au, for the DA and AD photocells, but could not find any systematic dependence of photocurrent on the work function of the used metal electrodes (Fig. S3, ESI†). This indicates that the polarity of the photocurrent in these Parylene-C MISIM photocells is primarily governed by the photo-induced polarization in the S layer.

3.2 Frequency dependent phenomena and rate-determining process in MISIM photocells

We examined the dependence of the photocurrent for the DA and AD photocells on the light-on–off modulation frequency in the range from 1 kHz to 1 MHz. The results for the DA and AD photocells are shown in Fig. S4 and S5, respectively (ESI†). Fig. S2 (ESI†) shows the time trajectory of the light intensity in

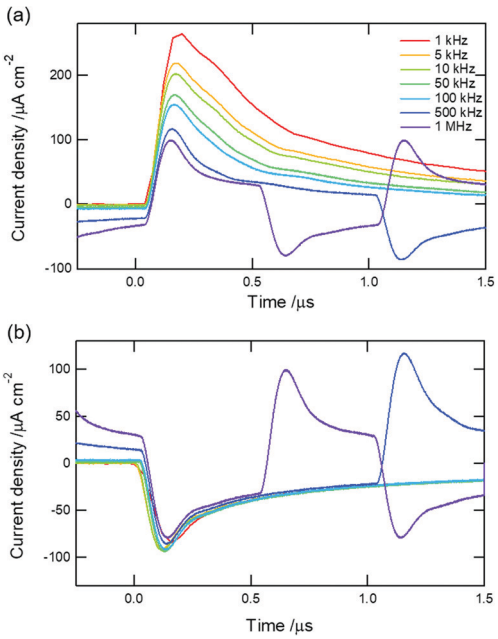

Fig. 3 Time trajectories of the photocurrent for the DA photocell at various frequencies under illumination (a) and in the dark (b).

this frequency range, indicating nearly square-shaped periodic signals with 50% duty-cycle. Fig. 3(a) and (b) show the frequency dependence of the time trajectories of the photocurrent in the DA photocell at various frequencies, in which the illumination-on and -off starts at $t = 0$, respectively. As can be seen, the ON current under illumination in Fig. 3(a) depends significantly on the modulation frequency; the current peak decreases with increasing frequency. In contrast, the curvature of the OFF current in the dark, shown in Fig. 3(b), depends little on the frequency. Thus, there is a crucial difference between the polarization process under illumination and the depolarization process in the dark. The AD photocell shows nearly the same results (see Fig. S6, ESI†): a significant frequency dependence of the ON current and little dependence of the OFF current. Thus, the observed dependence on modulation frequency does not depend on current polarity.

We calculated the time dependence of the polarization change ΔP for the DA photocell at various frequencies by integrating the ON and OFF currents with respect to time (Fig. S7 and S8, ESI†). It is notable that, at each frequency, the maximum values of $|\Delta P|$ in the illumination-on and -off states are nearly the same, indicating that the leakage currents in these devices should be negligible. Fig. 4(a) shows the results for the polarization process under illumination. When the illumination starts at $t = 0$, the values of ΔP at all frequencies show a rapid increase followed by a gradual saturation, with decreasing saturation values of ΔP with increasing frequency. Fig. 4(b) shows the time dependence of ΔP in the dark, indicating exponential decay dependencies in the polarization process. Interestingly, the curvatures of the ΔP traces at the measured frequencies completely coincide with each other. It can thus be considered that the initial state of depolarization, which corresponds to the final state of polarization, does not

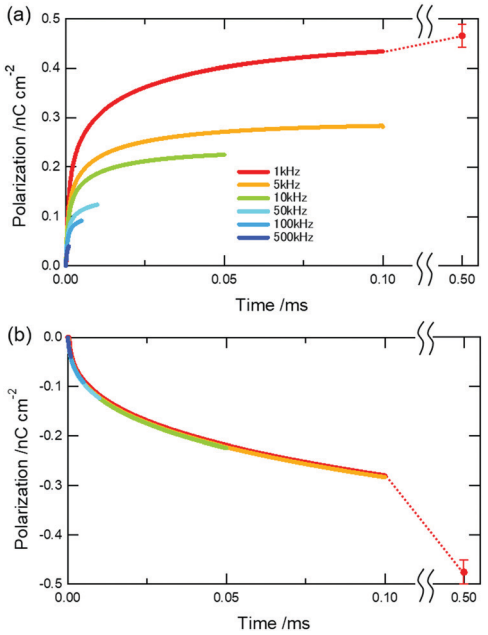

Fig. 4 Time dependence of the polarization change ΔP for the DA photocell at various frequencies under illumination (a) and in the dark (b).

significantly depend on frequency, whereas the initial state of polarization, which corresponds to the final state of depolarization, does depend on frequency. Fig. S9 (ESI†) shows the results for the AD photocell, which are essentially the same as those for the DA photocell.

These findings can be well-explained by assuming a fast polarization under illumination and a slow depolarization in the dark. Fig. 5 schematically depicts the expected oscillations of the polarization in the modulation cycles under illumination of a given light intensity, and indicates the dependence on the modulation frequency, under the stated assumption. In the case of a low modulation frequency (blue), the degree of polarization would reach 100% (for a given light intensity) because of a quick polarization, and it can revert to 0% in the dark because the modulation rate is very slow. This represents the situation at the modulation frequency of 1 kHz. In the case of a high modulation frequency (red), the eventual degree of polarization would approach 100% under illumination because of the high polarization rate but cannot revert to 0% in the dark because of the slow depolarization. In this case, the next polarization process starts from an intermediate degree of polarization, *e.g.*, 70%, so that the polarization would oscillate between 70 and 100%. This is considered to correspond to the situation at 1 MHz. In the case of an intermediate modulation frequency (green), the polarization oscillates between, *e.g.*, 40 and 100%, which would correspond to the situation at 10 kHz. It is interpreted that, as shown in Fig. 4(b), the depolarization processes depend little on the modulation frequency, because they correspond to relaxations from approximately the same state, namely from the state of 100% polarization for a given light intensity. We estimated the saturation value ΔP_{sat} of ΔP from the data at 1 kHz, as well as the maximum value ΔP_{max} of ΔP at each frequency. Fig. S10 (ESI†) shows the frequency dependence of $\Delta P_{max}/\Delta P_{sat}$, which corresponds to the width of the polarization oscillation. With an increase in modulation frequency from 1 kHz, the values of $\Delta P_{max}/\Delta P_{sat}$ quickly decrease, but above 100 kHz, the decrease becomes less significant. The results for the AD photocells are described in the ESI,† and they are essentially the same as those for the DA photocell.

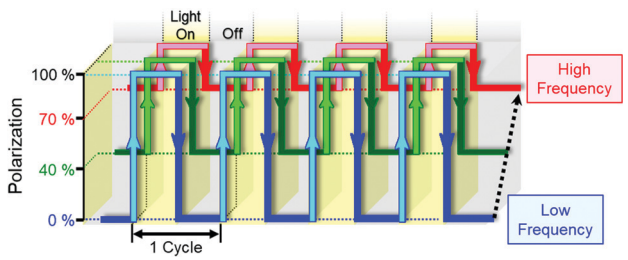

Fig. 5 Schematic explanation of the polarization oscillation between the partially and fully polarized states.

The optoelectronic conversion in the DA and AD photocells under illumination is considered to consist of three steps: (i) exciton generation and their migration to the D|A interface, (ii) charge separation at the D|A interface, and (iii) hole and electron migration towards the I|D and I|A interfaces, respectively, resulting in device polarization. In the dark, three reverse steps would take place to relax the polarization: (iv) hole and electron migration to the D|A interface, (v) charge recombination, and (vi) relaxation to the ground state. It is widely recognized that the rates of exciton migration (i) and relaxation (vi) and those of charge separation (ii) and recombination (v) are much faster than the dynamic range shown in Fig. 4. This means that the rate-determining steps in the observed polarization and depolarization processes are ascribable to the carrier migration under illumination (iii) and in the dark (iv), respectively. It can be concluded from this study that the carrier migration under illumination is much faster than that in the dark.

One possible explanation for the observed difference between the carrier migration rates under illumination and in the dark would be as follows. When the illumination is turned on, the charge carrier density would be very high at the D|A interface, resulting in a negative gradient from this interface to the I layers, since charges can be expected to be generated predominantly at the D|A interface in the present device architectures. This gradient results in a diffusion potential that would support the migration of carriers from the D|A interface to the I layers, thus generating a displacement current in the outer circuit. This gradient becomes less steep during the illumination period, reducing the diffusion potential with time. When the illumination is turned off, charge recombination takes place at the D|A interface, resulting (eventually) in a positive gradient of carrier density from the D|A interface to the I layers. This supports the migration of carriers towards the D|A interface leading to a displacement current of opposite sign, due to depolarization of the S layer. Clearly, the positive gradient in the dark would be smaller than the negative gradient generated under illumination. This explanation does not include the effect of any built-in fields within the device (not just from the outer electrodes), which would lead to a drift

component to the carrier migration. Furthermore, another important factor that should be considered is the effect of carrier trapping. Continuous carrier generation would serve to replace carriers that become localized in traps, ensuring a fast polarization of the S layer. However, in the dark, no further carrier generation occurs, thus the rate of depolarization would be limited by the timescales of de-trapping, since all carriers moved under illumination should recombine in order to fully depolarize the S layer. It is notable that a fast rise and slow decay of photocurrent has also been observed in organic phototransistors, which has been related to the presence of trap sites in the depletion region.[27] One strategy to balance the charge migration rates in the MISIM devices would therefore be to operate the device under background illumination. This has been demonstrated by Reissig *et al.* for MISM devices, where a greater symmetry for the light on/off processes, and faster rise and fall times for the transient waveforms were found under background illumination.[16] To better understand the relative contributions of carrier drift, diffusion and trapping, as well as how these are affected by any pre-polarization within the constituent layers of the MISIM architecture, such experiments on the present devices should further be supported by computer modeling including drift/diffusion simulations. In order to improve the detectivity and bandwidth of our devices under on–off illumination, specific strategies to improve the rate-limiting step of the migration of holes and electrons in the S layer in the dark should be targeted.

4. Conclusion

We investigated MISIM photocells consisting of Parylene C as the I layers and ZnPc-C_{60} bilayers as the S layer. The current polarity was governed by the ZnPc-C_{60} sequence in the S layer rather than by the potential difference between the electrodes; the polarization induced by the donor–acceptor charge-transfer, following excitation, determined the polarity. Modulated illumination (1 kHz–1 MHz) of the MISIM photocells induced the alternation of polarization and depolarization in the S layer, which was completely isolated from the metal electrodes (M layers), and resulted in the generation of an AC polarization current in the outside circuit. However, with an increase in modulation frequency, the polarization current monotonically decreased; the photocurrent at 1 MHz was only one-tenth of that at 1 kHz. The characteristic frequency dependence of the photocurrent appeared only during illumination, and the time trajectories of the dark current depended little on the frequency. This can be well-explained by an imbalance between the fast rates of polarization under illumination and the slow depolarization in the dark. Therefore, it is necessary to improve the speed of this identified rate-determining process, *i.e.*, the depolarization in the dark, to realize high-speed photodetectors and photosensors based on the MISIM architecture.

Conflicts of interest

There are no conflicts to declare.

Acknowledgements

This study was supported by the Japan Society for the Promotion of Science (JSPS) KAKENHI Grants (no. JP16H06353 and JP18H04482) and by the JSPS Bilateral Collaboration. We are grateful to the Ministry of Education, Culture, Sports and Technology (MEXT) of Japan for a Grant-in-Aid for Young Scientists to SD (16K17971) and LR (16K17853).

References

1 S. R. Forrest, *Nature*, 2004, **428**, 911–918.
2 M. Graetzel, R. A. J. Janssen, D. B. Mitzi and E. H. Sargent, *Nature*, 2012, **488**, 304–312.
3 S. Günes, H. Neugebauer and N. S. Sariciftci, *Chem. Rev.*, 2007, **107**, 1324–1338.
4 J.-P. Correa-Baena, A. Abate, M. Saliba, W. Tress, T. Jesper Jacobsson, M. Grätzel and A. Hagfeldt, *Energy Environ. Sci.*, 2017, **10**, 710–727.
5 P. W. M. Blom, V. D. Mihailetchi, L. J. A. Koster and D. E. Markov, *Adv. Mater.*, 2007, **19**, 1551–1566.
6 T. Kirchartz, T. Agostinelli, M. Campoy-Quiles, W. Gong and J. Nelson, *J. Phys. Chem. Lett.*, 2012, **3**, 3470–3475.
7 J. G. Tait, U. W. Paetzold, D. Cheyns, M. Turbiez, P. Heremans and B. P. Rand, *ACS Appl. Mater. Interfaces*, 2016, **8**, 2211–2219.
8 A. Armin, R. D. Jansen-vanVuuren, N. Kopidakis, P. L. Burn and P. Meredith, *Nat. Commun.*, 2015, **6**, 6343–6351.
9 Y. Yao, Y. Liang, V. Shrotriya, S. Xiao, L. Yu and Y. Yang, *Adv. Mater.*, 2007, **19**, 3979–3983.
10 S. Ullbrich, B. Siegmund, A. Mischok, A. Hofacker, J. Benduhn, D. Spoltore and K. Vandewal, *J. Phys. Chem. Lett.*, 2017, **8**, 5621–5625.
11 L. Hu, Y. Noda, H. Ito, H. Kishida, A. Nakamura and K. Awaga, *Appl. Phys. Lett.*, 2010, **96**, 243303.
12 S. Dalgleish, M. M. Matsushita, L. Hu, B. Li, H. Yoshikawa and K. Awaga, *J. Am. Chem. Soc.*, 2012, **134**, 12742–12750.
13 B. Li, S. Dalgleish, Y. Miyoshi, H. Yoshikawa, M. M. Matsushita and K. Awaga, *Appl. Phys. Lett.*, 2012, **101**, 173302.
14 L. Hu, X. Liu, S. Dalgleish, M. M. Matsushita, H. Yoshikawa and K. Awaga, *J. Mater. Chem. C*, 2015, **3**, 5122–5135.
15 L. Reissig, K. Mori, R. Treadwell, S. Dalgleish and K. Awaga, *Phys. Chem. Chem. Phys.*, 2016, **18**, 6821–6830.
16 L. Reissig, S. Dalgleish and K. Awaga, *AIP Adv.*, 2016, **6**, 015306.
17 T. Miyasaka and T. N. Murakami, *Appl. Phys. Lett.*, 2004, **85**, 3932–3934.
18 T. Miyasaka and T. N. Murakami, *Appl. Phys. Lett.*, 2005, **86**, 196102, Response to Comment on [*Appl. Phys. Lett.*, 2005, **86**, 196101].
19 L. Reissig, S. Dalgleish and K. Awaga, *Sci. Rep.*, 2018, **8**, 15415.
20 W. J. Wang, C. X. Shan, H. Zhu, F. Y. Ma, D. Z. Shen, X. W. Fan and K. L. Choy, *J. Phys. D: Appl. Phys.*, 2010, **43**, 045102.
21 G. M. Ali and P. Chakrabarti, *J. Phys. D: Appl. Phys.*, 2010, **43**, 415103.

22 A. Perumal, M. Fröbel, S. Gorantla, T. Gemming, B. Lüssem, J. Eckert and K. Leo, *Adv. Funct. Mater.*, 2012, **22**, 210–217.
23 A. Perumal, B. Lüssem and K. Leo, *Appl. Phys. Lett.*, 2012, **100**, 103307.
24 M. Fröbel, T. Schwab, M. Kliem, S. Hofmann, K. Leo and M. C. Gather, *Light: Sci. Appl.*, 2015, **4**, e247.
25 Y. Kinoshita, T. Hasobe and H. Murata, *Jpn. J. Appl. Phys.*, 2008, **47**, 1234–1237.
26 B. Yu, L. Huang, H. Wang and D. Yan, *Adv. Mater.*, 2010, **22**, 1017–1020.
27 B. Mukherjee, M. Mukherjee, Y. Choi and S. Pyo, *J. Phys. Chem. C*, 2009, **113**, 18870–18873.